Lawrence Berkeley National Laboratory
Earth & Environmental Sciences

Title
Modelling the water injection induced fault slip and its application to in-situ stress estimation

Permalink
https://escholarship.org/uc/item/85t0638t

Authors
Shiu, Wenjie
Guglielmi, Yves
Graupner, Bastian
et al.

Publication Date
2021

DOI
10.1016/j.ijrmms.2020.104537

Peer reviewed

Modelling the water injection induced fault slip and its application to in-situ stress estimation

Wenjie Shiu[1*], Yves Guglielmi[2], Bastian Graupner[3], Jonny Rutqvist[2]

[1]SINOTECH Engineering Consultants, INC, Taiwan

[2]Lawrence Berkeley National Laboratory, Berkeley (LBNL), U.S.A.

[3]Swiss Federal Nuclear Safety Inspectorate (ENSI), Brugg, Switzerland

* Corresponding author. Tel.: +886-2-8791-9198, fax.: +886-2-8791-2198
  E-mail address: wshiu@sinotech.org.tw (W. Shiu)

ABSTRACT:

Fault reactivation due to water injection is assessed within the scope of nuclear waste disposal design. A model using the distinct element method is applied to reproduce the fault reactivation during an experiment carried out at the Mont Terri Underground Research Laboratory in Switzerland. A conceptual model is first presented to understand the hydro-mechanical coupling behavior between water pressure and rock joint movement. The model simulations show that the dominant factors on fault slip are shear stress and frictional resistance. Moreover, modeling shows that fault reversible opening in the normal direction occurs first at a lower pressure, whereas shear displacement as a result of shear slip is produced once a sufficiently high pressure is reached. We demonstrate that a coupled numerical analysis of the rock displacement trend and fluid pressure measured at the injection point allow an in-situ estimation of the full stress tensor.

Keywords: fault reactivation; hydro-mechanical coupling; in-situ stress estimation

Highlights

- Fault reactivation due to injection of water pressure;
- Fully hydro-mechanical coupling using the Distinct Element Method;
- *In-situ* stress estimation based on the rock displacement trend during the fluid injection test;
- Flow connection between two elements via crack propagation.

1 INTRODUCTION

Fault reactivation or shearing of fractures can be an important issue related to the safety of deep geological disposal for radioactive waste [1, 2, 3]. Elevated risk may arise when fault reactivation is triggered, leading to an increase in permeability and a potential flow path for transport of radionuclides, if released from waste package. It is well-known that the key factors triggering the fault slip are shear stress and the magnitude of frictional resistance [4]. Different models for reproducing the behavior of fault reactivation have been proposed [5, 6, 7]. However, the understanding of relevant hydro-mechanical response to fault reactivation is still limited.

In the present work, a *3DEC* model [8] based on the Distinct Element Method (DEM) is applied to simulate the coupled hydraulic and mechanical behavior during fault reactivation triggered by water injection. The simulation work was conducted as part of the DECOVALEX (DEvelopment of COupled models and their VALidation against EXperiments) project, an international research and model comparison collaboration for understanding and modeling of coupled thermo-hydro-mechanical-chemical processes in geological systems [9]. The current phase is DECOVALEX-2019 running from 2016 through 2019, and this study falls under Task B entitled 'Modeling the induced slip of a fault in argillaceous rock' [10]. The main objectives of Task B included interpretative modeling of fault reactivation experiments carried out at the Mont Terri Rock Laboratory in Switzerland [11-13]. The mechanical response of the fault is represented by a Coulomb slip material, whereas two flow models are used to reproduce hydraulic behavior of different nature of the fault. A fully coupled hydro-mechanical calculation, used for the present study, is based on the fast-flow logic implemented in *3DEC* [8].

The in-situ experiment considered in this study is a controlled fault activation experiment involving fluid pressurization of the borehole that eventually induces failure starting from the borehole wall. In some aspects it is analogous to hydro-fracturing stress measurements which also involves high-pressure injection to break the rock and reopening fractures at the borehole wall [14-16]. The conventional hydro-fracturing stress measurement method involves forming new fractures under high injected water pressure, whereas an alternative and less common method is to reopen pre-existing fractures [14]. The experiment setting used in the present work corresponds to the second method. The stress measurement from Hydraulic Tests on Preexisting Fractures (HTPF) is first presented by Cornet and Valette [17] and has been practiced for the last 30 years [17-19]. The idea is to deduce the rock stress according to the amount of normal stress supported by fractures and the magnitude of pressure needed to open a fracture intersecting the well. The latter quantity is

denoted the "fracture opening pressure" (FOP) which may be determined from constant rate injection or step rate injection tests [14, 18]. A challenge is the relatively large number of tests (up to 18-20 tests) necessary for determining the complete stress tensor, and the assumption that the FOP relates to pure fault opening.

The objective of DECOVALEX-2019, Task B is to develop, compare and validate models for fault activation relevant to deep underground nuclear waste disposal. Based on the fault reactivation experiment carried at the Mont Terri underground rock laboratory in Switzerland, a *3DEC* numerical model is conducted to interpret the findings of the experiment. The following issues will be addressed in the present work: (1) to understand the mechanism of the fault reactivation and the associated coupling behavior between injected water pressure and fault movement; (2) to estimate the principal stresses based on the rock displacement and the magnitude of injected pressure. A two-step modeling process is conducted related to steps defined in the DECOVALEX-2019, Task B, but with the aim of estimating the in-situ stress. Step 1 relates to a conceptual model for inspection of the coupling behavior between water injection and fault reactivation. According to the findings on Step 1 modelling, the configuration of Step 2 modeling is adjusted to achieve the in-situ stress estimation. The results of step 2 modeling are compared and discussed with experimental data from the Mont Terri Laboratory.

2 EXPERIMENT SETTING

The numerical model aims at reproducing the fault reactivation experiments performed at Mont Terri underground research laboratory [11-13]. An overview of the experimental setting is provided in Fig. 1. The experiment explores the couplings between fault reactivation in an indurated clay host rock and the potential enhanced fluid displacement through a previously low-permeability formation. The experiments were conducted using the unique SIMFIP (Step-Rate Injection Method for Fracture In-Situ Properties) borehole deformation tool [22]. The borehole interval is selected using an optical televiewer logging tools in a way that the injection chamber is intersected by pre-existing fractures. The interval is then isolated with inflatable packers and the isolated zone is pressurized with water. The displacements at high sampling rate (~500 Hz) are monitored in three dimensions, which allows one to reconstruct both normal and shear fault movements. Such approach can be used to determine the *in-situ* profile of natural fractures permeability and deformability characteristics of normal and shear stiffness. Seismic sensors were also installed close to the experiment to determine if fault reactivation could eventually produce microseismic events.

A total of five injection tests were conducted beneath, within and above the main fault during the two measurement campaigns of June and October/November 2015. A second SIMFIP probe was used to reveal the connectivity response between BFS2 (injection borehole) and BFS1 (monitoring borehole). During all tests, pore pressure was also monitored at three locations around the main fault (borehole BFS4, 5 and 6). Induced seismicity was monitored at borehole BFS3 at two depths 43.9m (Main fault footwall) and 35.9m (main fault hanging wall damage zone). All measurements were synchronized. The current study is related to injection test performed at the packed-off section at 37.2 m depth of borehole BFS2 with a breakthrough and pressure monitoring at BFS4 located 1.5 m away. The borehole is pressurized in a step wise manner from 0.5 MPa to 6.3 MPa over 800 seconds (see Fig. 1b). The same injection protocol is used in the numerical model.

(a)   (b)
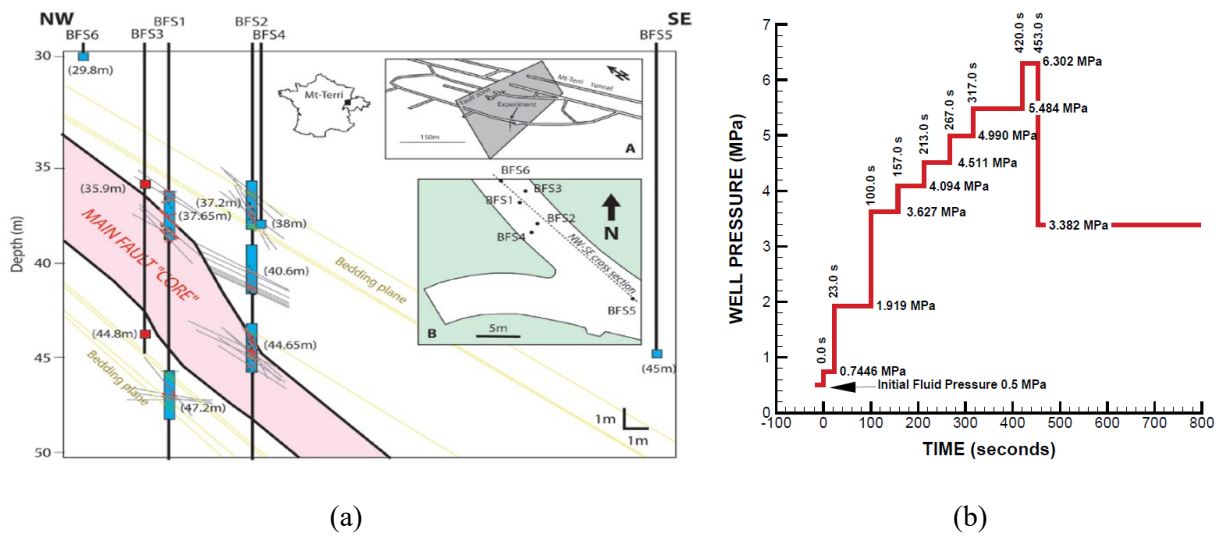
Figure 1: (a) Mont Terri main fault with the location of the experiment and cross section of the main fault with the location of the packed-off sections [10]. (b) Water pressure injection time history used for fault reactivation experiment.

3 MODEL DESCRIPTION

A simple model geometry is used for Step 1 modeling: a cube of 20 m length representing the host rock with a single fracture of 65° dip angle. In order to better reproduce the model behavior during water injection induced fault reactivation, a smaller mesh size (0.25 m) is used for zones located right on the fault and nearby whereas a coarser mesh is used when moving away from the fault (Fig. 2). The following *in-situ* stresses are considered: minimum horizontal principal stress σ_{xx} = 3.3 MPa, intermediate horizontal principal stress σ_{yy} = 6.0 MPa and maximum vertical principal

stress σ_{zz} = 7.0 MPa. Initial pore press is set to 0.5 MPa and no stress gradient is considered. Table. 1 gives the relevant parameters used for fault, rock and fluid. Note that the host rock is assumed to be elastic and impermeable. Thus, fluid flow is only allowed within the fault plane. Two fault models are studied [10] (referred as FM1 and FM2 in Tab. 1):

- FM1: Fluid flow takes place between two elements where mechanical failure is detected (according to the Coulomb slip failure criteria). In order to allow the fluid flow to take place during the early injection period, some initial cracks are introduced around the injection point within a circle of 0.7 m radius. Note that elements located beyond this predefined region are in full contact. Thus, no fluid flow is allowed at the outer region before formation of new cracks. This flow model can be used to simulate a fault with filling material.
- FM2: Fluid flow is available freely over the entire flow plane without regarding the failure status of joint elements. This flow model can be used to simulate an already opened fault.

(a)   (b)
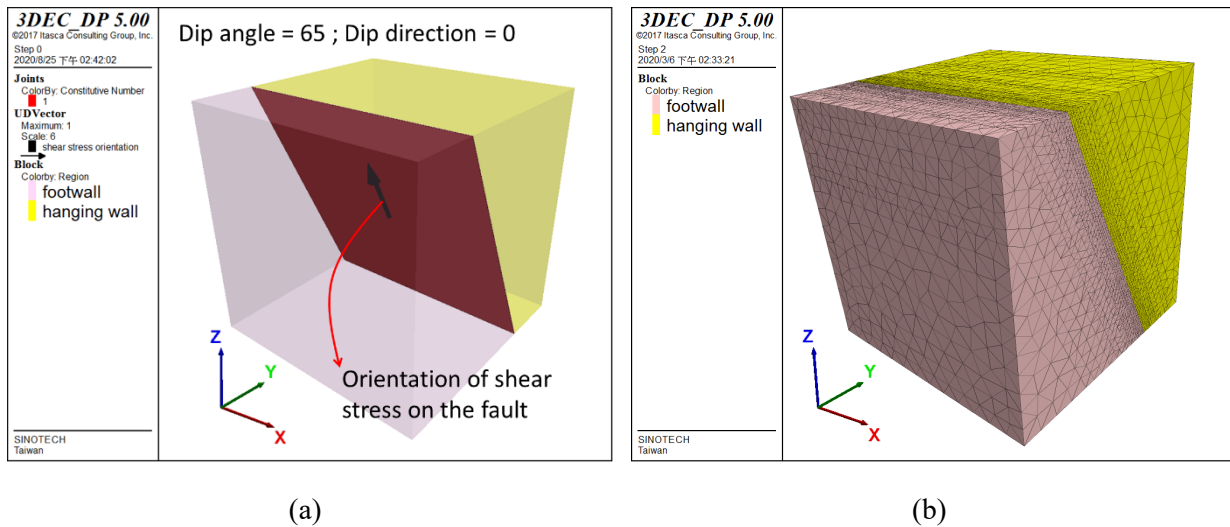
Figure 2: (a) Geometric representation of the conceptual model. (b) Mesh discretization.

The radius of the initial fractured zone is given as 0.5 m as an input data for Task B. While in reality a mesh size of 0.25 m was used to discretize the whole flow plane, which resulted in fewer flow nodes to be presented along a flow path between the injection point and the boundary of the initial fractured zone. In order to allow more flow nodes to be presented initially inside the fractured zone and to better reproduce the pressure propagation, the range of radius for the initial fractured zone is expanded from 0.5 m to 0.7 m.

For the joint fluid flow computation, we assume that the flow goes through two parallel plates. The distance between these two plates is the hydraulic aperture, u_h. The flow rate, q_i, per unit width between plates (or aperture) may be written by the cubic law [23]:

$$q_i = -\frac{u_h^3 \rho g}{12\mu} \emptyset_{,i} = -k_H \emptyset_{,i} \tag{1}$$

where μ is the fluid viscosity [Pa s], ρ is the fluid density [kg/m³], g is the gravity acceleration [m/s²], $\emptyset_i$ is the hydraulic head [m], and k_H is the hydraulic conductivity [m²/s].

The hydraulic aperture of the fault plane is given by

$$u_h = u_{h0} + \Delta u_n \tag{2}$$

Where u_{h0} is the initial hydraulic aperture and Δu_n is the joint normal displacement increment.

Note that, two sets of aperture parameters are listed in Tab. 1: initial aperture and initial creation aperture. In *3DEC*, there is no difference between them. They are treated as initial hydraulic aperture (u_{h0}) in fluid flow computation. The change in joint normal displacement comes from two contributions: due to the change in effective normal stress (Δu_e, elastic part) and the contribution from joint dilation (Δu_p, plastic part):

$$\begin{aligned} \Delta u_n &= \Delta u_e + \Delta u_p \\ \Delta u_e &= \Delta \sigma_n'/k_n \\ \Delta u_p &= u_s \times tan\varphi \end{aligned} \tag{3}$$

where $\Delta \sigma_n'$ is the change in effective normal stress, k_n is the joint normal stiffness, u_s is the plastic shear displacement and φ is the dilation angle. Note that, the contribution from dilation takes place only when joint is slipping. Thus, u_s represents the shear displacement after onset of slip.

The fluid pressure in the fracture affects the fracture normal deformation. When the rock fracture is filled with fluid under a certain pressure, P_p, the normal deformation of the fracture is a function of a linear combination of the confining pressure in the rock, σ_n, and the fluid pressure:

$$\sigma_n' = \sigma_n + \alpha P_p \tag{4}$$

The effective stress coefficient, α, can be measured experimentally to be in the range of $0.5< \alpha <1.0$, small α for rough surface and large α for smooth surface. In *3DEC*, when the effective stress is used for assessment of normal or shear strength of rock fractures, which is the case in this study, the effective stress coefficient is always equal to 1.

The pressure change in flow element is computed by:

$$p = p_0 + K_\omega Q \frac{\Delta t}{V} - K_\omega \frac{\Delta V}{V_m} \tag{5}$$

Where p and p_0 are respectively final and initial pore pressure, K_ω is the fluid bulk modulus [Pa], Q is the sum of flow rates [m³/s] into the flow element from all surrounding contacts and Δt is the time step. V, ΔV and V_m are respectively current flow element volume [m³], volume change in the current step and the average volume.

In *3DEC* model, the fault plane is explicitly represented by a planar joint element. A joint element can be further discretized into a series of triangle meshes, denoted as sub-contacts. In the coupling process, the effective stress are updated at each sub-contact, accounted for the amount of change in pore pressure. The mechanical failure state is then verified according to the associated constitutive model assigned on the joint element. In this study, the Coulomb slip law is applied to reproduce the shear behavior of the fault. The sub-contacts satisfy the Coulomb slip failure condition will be assigned a failure indicator equal to 1 (indicating that they have already failed), while the indicator for the intact sub-contacts are equal to zero. It is clear that both mechanical and hydraulic responses affect the flow element pore pressure. Note that, the same governing equations are used for FM1 and FM2 models to compute relevant hydraulic (flow rate and pore pressure) and mechanical responses (force and displacement). The only difference is that the contact failure state is checked before the fluid flow computation between two connecting sub-contacts if FM1 model is applied. Thus, flow only occurs within the portions of flow planes where the associated sub-contacts are failed. Whereas for FM2 model, the previous verification is skipped, *i.e.*, flow will occur in all planes.

Fig. 3 shows the Coulomb slip mechanism of the fault due to changes in pore pressure. The Coulomb slip failure envelope can be approximated from joint strength properties (friction angle, cohesion and tensile strength). Before the water injection, the fault itself is in equilibrium under a

given initial stress state. When injection starts, the effective normal stress decreases with the increase in pore pressure, whereas the shear stress remains unchanged. Thus, the stress path moves horizontally toward the left direction during the injection (Fig. 3). When injected fluid pressure is high enough, the normal stress may touch the envelope and the slip is triggered (shear failure). The increment of FOP can be defined as the horizontal distance between the initial stress and the shear failure curve (denoted as Pc on Fig. 3). Theoretically, assuming that the fault reactivated in pure shear, it is possible to estimate the FOP if the fault properties and the initial joint stress data are available.

Table 1. Parameters for Fault, Host Rock and Fluid [10].

Material	Parameter	Value	
		FM1	FM2
Fault (Elasto-Plastic)	Normal Stiffness, kn (GPa/m)	20	20
	Shear Stiffness, ks (GPa/m)	20	20
	Cohesion (MPa)	0	0
	Friction Angle (°)	22	22
	Dilation Angle (°)	0	10
	Tensile Strength (MPa)	0	0
	Initial Aperture (µm)	28	10
Host Rock (Elastic)	Bulk Modulus, K (GPa)	5.9	5.9
	Shear Modulus, G (GPa)	2.3	2.3
	Density (kg/m3)	2450	2450
	Permeability	0	0
Fluid	Density (kg/m3)	1000	1000
	Compressibility (Pa-1)	4.4E-10	4.4E-10
	Viscosity (Pa s)	1E-3	1E-3
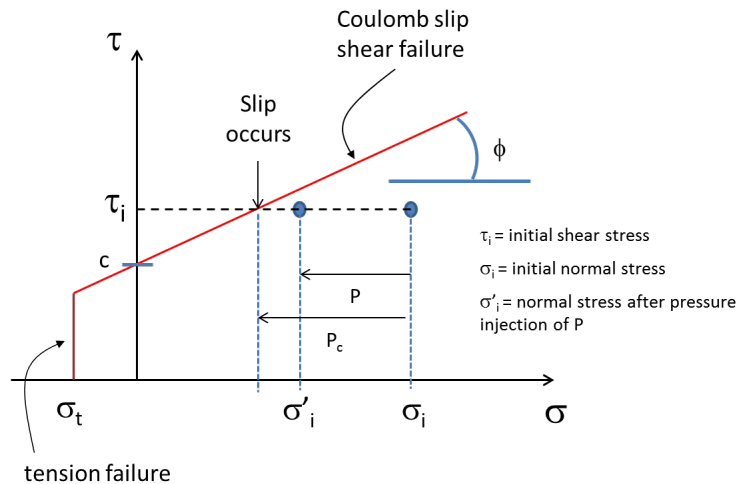
Figure 3: Schematic representation of Coulomb slip mechanism due to change in pore pressure.

4 RESULTS AND DISCUSSION

A two-step modeling sequence is conducted:

Step1: Inspection of coupling behavior between water injection and fault reactivation using conceptual model (see Fig. 2). Both FM1 and FM2 are performed.

Step2: According to the results obtained from Step1, an interpretative modeling is produced. The numerical results are compared with the experimental data.

4.1 *Step1 - FM1 results*

Fig. 4 gives the evolution of stress and displacement at the injection point during stepwise injection simulation. The evolution of pore pressure is the same as the one used for the Step 2 experiment with the injection point is located at the center of the fault. It is worth to note that the increase in pore pressure is achieved progressively over the first 5 seconds at the beginning of each increasing step. This process is adapted to avoid any numerical instability due to an instantaneously change in pore pressure. As expected, the increase in pore pressure (gray line) results in a decrease in effective normal stress (blue line). According to the Coulomb Slip criterion, the allowable maximum shear stress (denoted as max shear stress in Fig.4a) can be obtained by $\sigma_{s,max} = \sigma_n \cdot tan\emptyset$. The slip is triggered when the maximum allowable shear stress (green line) is reduced to the same value as the in-situ shear stress (red line). For the FM1 model, the slip is triggered at approximately 420 seconds. At that time, a significant increase in shear displacement along dip direction is observed (see Fig. 4b). Note that, no shear displacement along strike is produced, since the movement of the joint shear displacement is dominated by the orientation of in-situ shear stress on the fault (see Fig. 2a).

Evolution of flow rate and of pore pressure at monitoring points are illustrated in Fig.5. For the FM1 model, the fluid flow takes place only between flow elements where relevant sub-contacts are failed. From 0 to 400 seconds, a flow rate "jump" is observed each time when pore pressure is increased to a higher level. The flow rate jump lasts few seconds and is reduced quickly to zero. These small amounts of fluid injected into the fault increase the pore pressure of the fault. When pore pressure reaches the target value, it can be kept at a constant pressure with zero fluid input. This indicates that no leakage occurs during this period. At 420 seconds, a nonzero flow rate is needed to maintain a constant injection pressure at the injection point. This corresponds to the rupture propagation scenario, as shown in Fig.6. Rupture propagation is initiated at roughly 420

seconds, leading to a larger flow region on the fault. It stops propagating after 450 seconds when pressure is reduced to a lower level. As shown on Fig.5b, pore pressure at the monitoring points remains fairly unchanged before 420 seconds. Thereafter, it increases in an instantaneous manner from 0.5 MPa to 5.7 MPa and drops to the same residual value as the one prescribed in the injection point. To sum up, hydro-mechanical coupling behavior is observed in the FM1 model with the slip condition on the fault following the Coulomb slip criterion. Increases in pore pressure yields decrease in normal stress, thus shear resistance is reduced. Slip is triggered when the injected pressure reaches 6.3 MPa. At the same time as the rupture propagation extends, there is a clear increase in shear displacement on the fault. The pressure response at the monitoring point is likely to be synchronized with the one prescribed at the injection point, when the flow connection between these two locations is established via crack propagation.

(a)   (b)
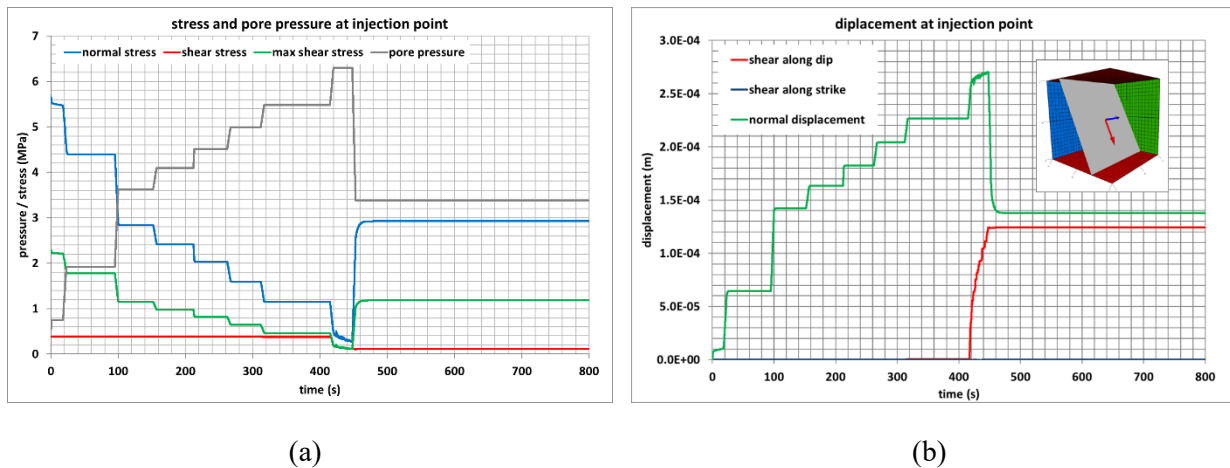
Figure 4: (a) evolution of stress and pore pressure at the injection point and (b) evolution of the displacements

(a)   (b)
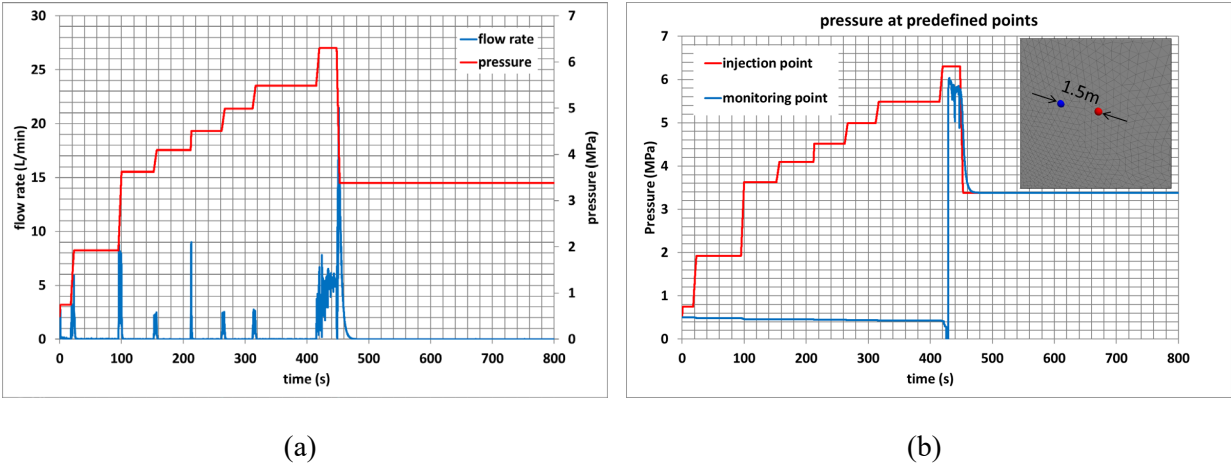
Figure 5: (a) evolution of flow rate and (b) evolution of pore pressure at monitoring points
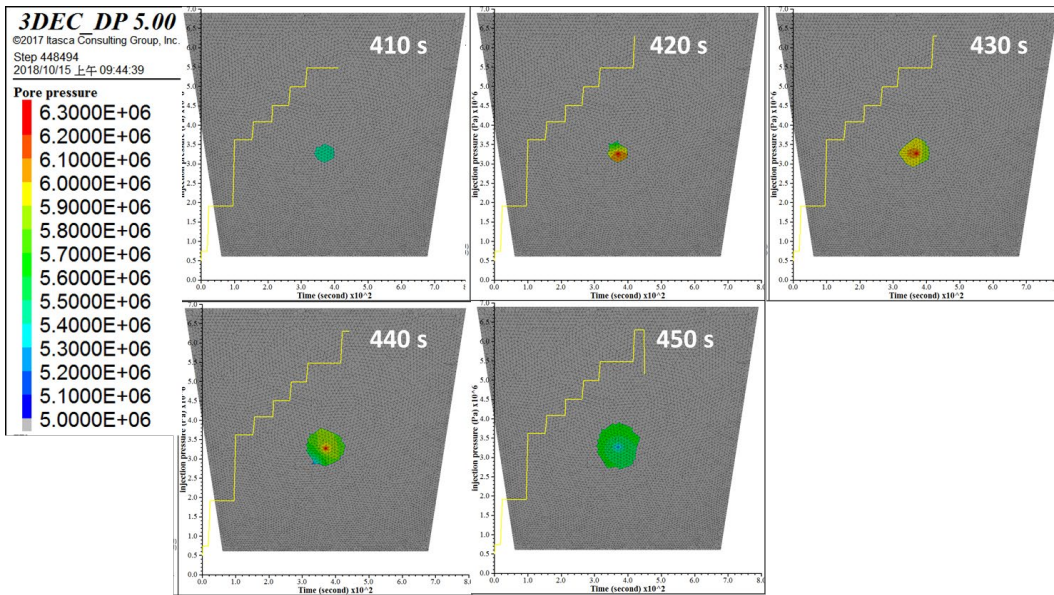
Figure 6: Contour of pore pressure on the fault at different time

4.2 *FM1 vs FM2*

Due to the different concept of fluid flow logic used for FM1 and FM2 models, the pore pressure contour behaves in a very different way (see Fig. 7). For the FM1 model, the fluid flow is initially limited within a small region around the injection point. The crack propagation takes place at 420 seconds. The allowable fluid flow region is expanded from 0.7 m radius to 1.6 m radius over the next 30 seconds. For the FM2 model, the fluid flow leaked across the entire flow plane, resulting in a smaller average pore pressure around the injection point. A higher flow rate at the injection point can be expected for the FM2 model to keep the pore pressure at the prescribed value (Fig.

8). Stress and displacement evolutions at the injection point are illustrated on Fig 9. A similar stress drop is observed for FM1 (solid curves) and FM2 (dotted curves), as they use the same stepwise pressure history. Logically, the same normal displacement is produced at the injection point (Fig. 9b). However, shear displacement produced by the FM1 model is much higher than for the FM2 model. In order to better understand the model behavior, a comparison of pore pressure profile along the fault dip direction is presented in Fig. 10. For the FM1 model, the injected water is accumulated within a small region (at 240 and 400 seconds). The pore pressure for elements inside this region is synchronously increasing, leading to a lower average normal stress and lower shear resistance. At 440 seconds, rupture propagation takes place and the high pore pressure region is extended from 0.7 m radius to 1.6 m radius. This implies that the sub-contacts located inside 1.6 m radius are failed. The pressure varies from the maximum value (6.302 MPa) at the injection point to the minimum value (close to 5.5 MPa) at the end-tip of 1.6 m radius. Thus, the FOP can be determined as the lower bound of high pore pressure region, *i.e.*, the value at the end tip of 1.6 m radius (FOP = 5.5 MPa). A meter-scale rupture area fault slip is produced, yielding a pronounced shear displacement. For FM2 model, the range of exceeding FOP is limited within 0.3 m radius (see dotted line at 440 seconds on Fig. 10), leading to a smaller shear displacement around the injection area. It is more difficult to trigger the fault reactivation over a sizeable area for FM2 model where the water leakage is allowed across the entire fault plane.
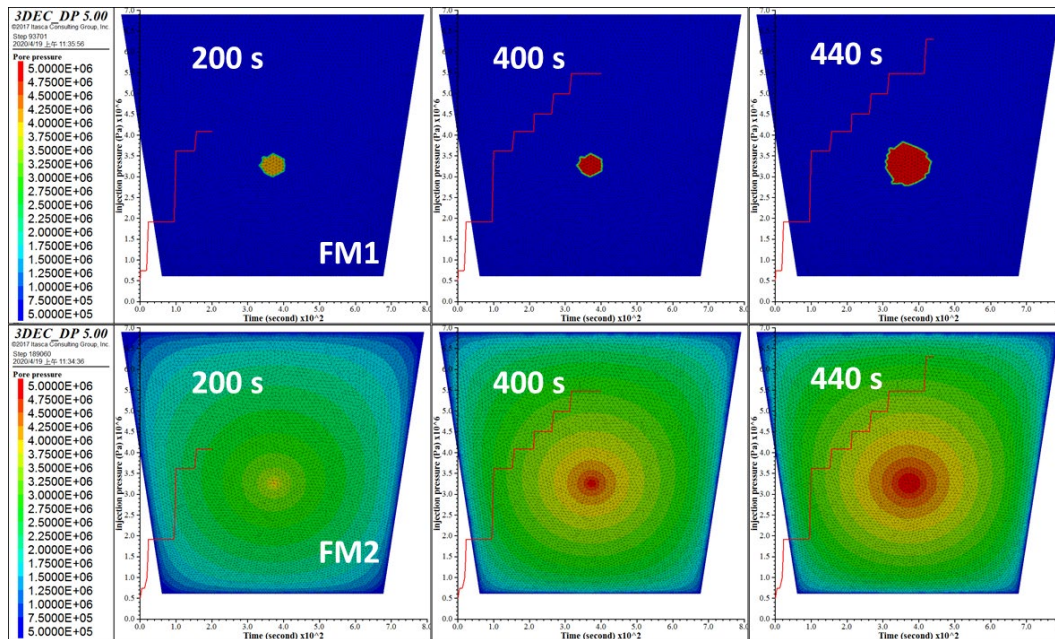
Figure 7. Pore pressure contour on the flow plane for FM1 and FM2.
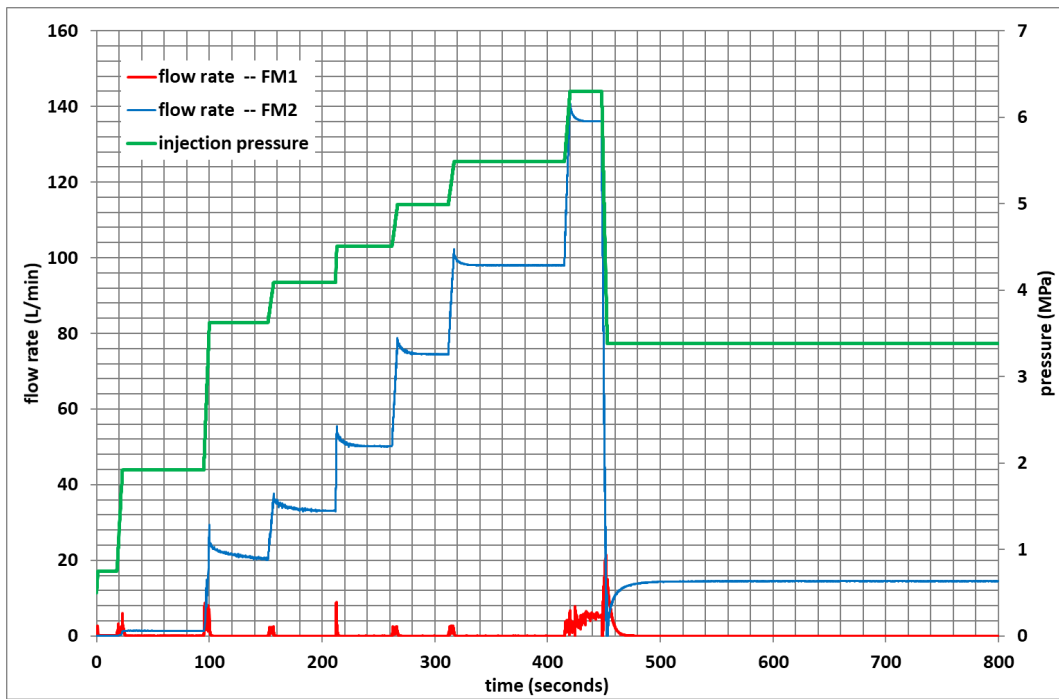
Figure 8: Evolution of flow rates measured at the injection point for FM1 and FM2.
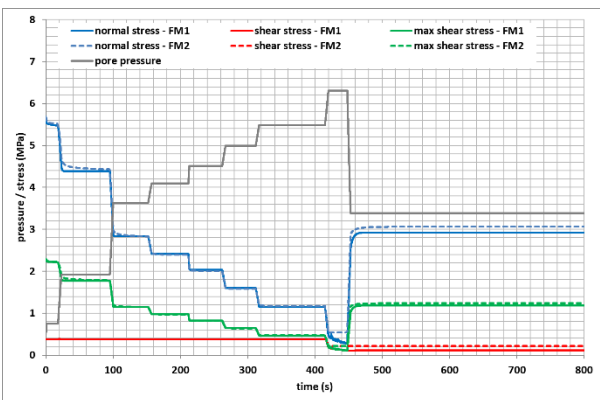
(a)
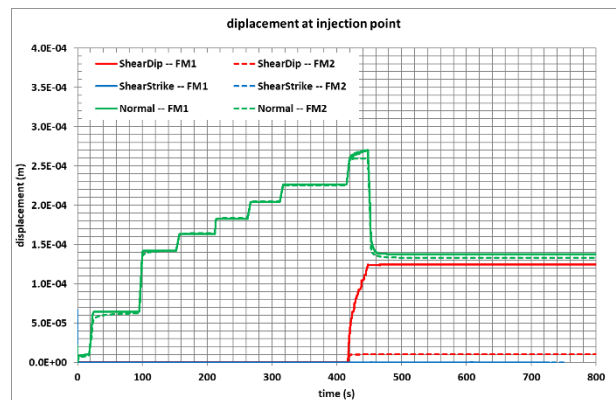
(b)

Figure 9. Comparison between FM1 and FM2 in terms of (a) Evolution of stress patterns and (b) displacement at the injection point.
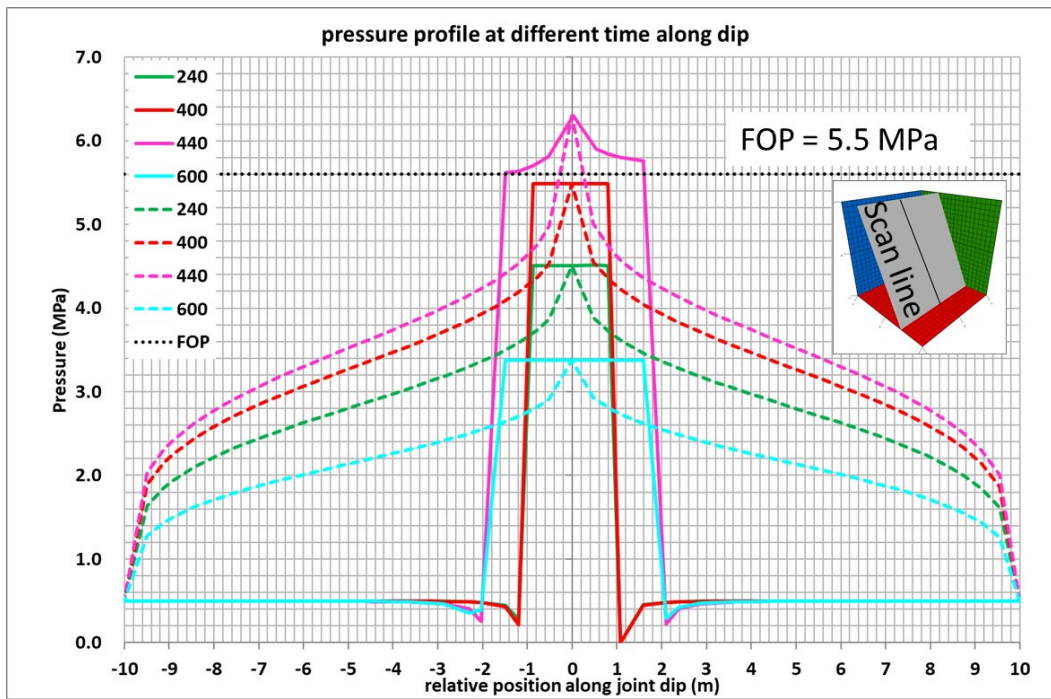
Figure 10: Pore pressure profile along joint dip for FM1 (solid line) and FM2 (dashed line) at different time.

4.3 *Discussion*

During the fault reactivation experiment test, the rock displacements were monitored at the injection point. These data can be further used in the interpretative modeling (Step 2). A similar representation of the FM1 model result is shown in Fig. 11, in terms of the trajectory of rock displacement. The concerning measurement location is very close to the injection point, as what has been monitored in the field experiment. The orientation of the maximum in-situ shear stress of the fault is also illustrated on the same figure. According to the displacement trend, it can be separated into 3 parts (blue, green and red). Each of them corresponds to different injection time interval:

Part 1: from 0 to 420 seconds, the injected water pressure has not yet reached FOP. Only joint normal displacement is produced. Thus, the rock displacement moves approximately normal to the fault.

Part 2: from 420 to 453 seconds, the injected water pressure exceeds FOP. Significant increase in joint shear displacement is observed. Therefore, the rock displacement changes its orientation and moves downward along the joint dip. Moreover, the orientation of the rock shear displacement follows the same direction as the fault *in-situ* maximum shear stress.

Part 3: from 453 to 800 seconds, the pore pressure decreases and the joint normal displacement reduces. Again, the rock displacement moves in a way parallel to the normal direction of the fault. Note that, the shear displacement remains unchanged (*i.e.* it is irreversible) during this period.
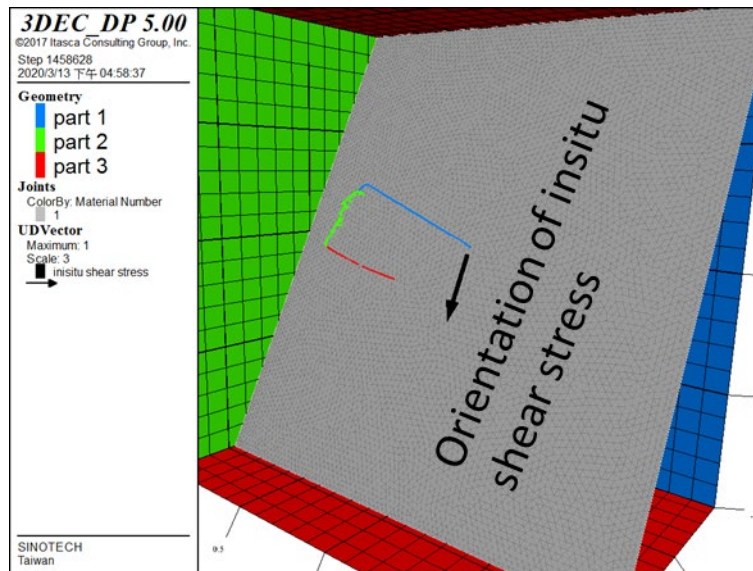
Figure 11: Trajectory of rock displacement close to the injection point, the black arrow denotes the orientation of in-situ maximum shear stress on the fault.

4.4 *Step 2: Interpretative modeling*

Based on Step 1 modeling results, the following approach is proposed for determination of the fault orientation and the in-situ stress.

Determination of the fault orientation: Fig. 12 gives the rock displacement near the injection point obtained from the experiment test. As discussed in the previous discussion, the measured trajectory can be further separated into three parts: part 1 for initial opening, part 2 for fault reactivation with obvious increase in shear displacement and part 3 after water pressure decrease. The fault orientation can be approximated in a way where the normal vector of the fault plane is parallel to the lineament of part 1 segment. The resulting orientation of the fault is as follow: dip angle=82° and dip direction=145° (see Fig. 12).

Determination of the in-situ stress: the *in-situ* stress applied on the model boundary (Fig. 13a) must satisfy the two following conditions. First, the projection of the part 2 behaviour on the fault $(\overrightarrow{V_{2p}})$ should yield the same unit vector as the one calculated from resultant fault shear stress $(\overrightarrow{V_{js}})$:

$$unit\left(\overrightarrow{V_{2p}}\right) = unit\left(\overrightarrow{V_{Js}}\right) \qquad (6)$$

Second, as shown on Fig. 13b, the horizontal distance between fault initial stress and Coulomb slip envelope should be close to the difference between FOP and initial pore pressure. Thus, the fault reactivation is forced to be triggered at the last injection step, when the injected water pressure reaches maximum value. In practice, the following procedure is used to determine the magnitude of the principal stresses. The stresses applied on the model boundary are adjusted in a way that the resultant shear stress on the fault satisfies the above-mentioned equation (6). A trial and error routine is needed to meet the previous condition. Then, the resultant fault normal stress and fault shear stress are plotted on the Coulomb slip diagram. The values of the boundary stresses need to be readjusted if the position of the stress state on the fault (red square on Fig.13b) is not close enough to the FOP line (dotted line on Fig. 13b). Besides, we must ensure that the equation (6) is still satisfied while readjusting the boundary stress values. This can be achieved by adding or removing the same amount of stress quantity to each principal stress component. As a result, the stress state can be drifted horizontally on the Coulomb slip diagram, and the orientation of the shear stress on the fault can remain unchanged.

In order to fulfill the previous conditions, the estimated *in-situ* principal stresses are: σ_H=5.8 MPa (at dip direction of 150), σ_h=4.9 MPa (fairly along fault strike) and σ_v =5.7 MPa (vertical). As indicated on Fig. 13b, the resulting shear stress on the fault is rather small (0.074 MPa). This can limit the development of shear displacement after the onset of fault reactivation. The *in-situ* stress state and the fault orientation are reported in Tab. 2. Comparing to the measured stress data from the site [24, 25], the orientation of the stress used in the model is slightly rotated by 5 degrees for the two horizontal components (see Fig. 13a). The previous setup is necessary to produce strike-slip shear displacement, as what has been shown on Fig. 12. After some pre-calibration works and investigation on experimental data, the following adaptation were made for the step 2 modelling: 1. The joint normal stiffness is increased from 20 GPa/m to 60 GPa/m. 2. Bulk modulus and shear modulus of host rock are set to 11.8 GPa and 4.6 GPa respectively. Other parameters are kept the same as those listed on Tab. 1. 3. According to the experiment observation, the tested fault near the injection area is likely to behave as a sealed fault with poor flow ability. The flow ability is further observed when the fault shear failure is triggered at high water injection pressure. Thus, only the FM1 method is used for Step 2 modeling since it predicts better model behavior according to previous *in-situ* observation.

Stress evolution at the injection point and comparison of displacement between numerical model and experimental data are reported in Fig. 14. As expected, the stress pattern follows the Coulomb criterion. The fault slip is triggered at roughly 420 seconds when maximum shear stress (green line) is reduced to the same amount as shear stress of the fault (red line). In general, the model shows reasonable displacement response comparing to the experimental data. A small amount of upward movement (positive vertical displacement in Fig. 14b) is captured by the model after the shear slip of the fault, since the major horizontal principal stress (5.8 MPa) is set a little larger than the vertical principal stress (5.7 MPa). The displacement data presented on Fig. 14b are measured in the global coordinates system, *i.e.*, western, northern and vertical. These data can be further represented by a 3D visualization (see Fig. 15a). The corresponding fault normal displacement and shear displacement are reported on Fig. 15b (projection of displacement trend on the fault). Overall, the displacement trend predicted by the model fits reasonably the one observed from the data. As expected, joint normal displacement increases with the increase in water pressure, during the initial fault opening stage. The increase in shear displacement appears at approximately 420 seconds, when the injected water pressure reaches 6.3 MPa. The timing of the fault reactivation is well captured, albeit a higher residual shear displacement (component along fault strike) is predicted by numerical model (18μm), comparing to the data (9μm). In fact, the fault shear displacement produced in the model remains unchanged after the water pressure step-down. However, the shear displacement of the data is reduced. This is also observed in the 3D visualization of displacement trend (Fig. 15a). The model shows a linear reduction in normal displacement along the normal of the fault, after pressure reduction. Whereas, the displacement trend of the data exhibits a small reverse behavior in shear component during the same period (black curve in Fig. 15a). A possible explanation could be that the rock wall damage is present in the injection chamber at high water pressures during experiment test. Moreover, both the displacement of rock matrix (including the damaged wall) and displacement of the fault are recorded by the sensors. Thus, the reverse in shear displacement could possibly be produced by the damaged borehole wall after unloading of water pressure, noting that in the numerical model the host rock is assumed to be elastic so such behavior wouldn't be captured. The shear behavior is mainly dominated by the orientation of the shear stress on the fault. The reverse in shear displacement can eventually occur only if the orientation of shear stress is reversed as well, which seems not be the case in the relevant injection test. What this implies is that the magnitude of the two horizontal stresses are very close to each other, thus rupture may preferentially develop along the weak preexisting fault surface. Nevertheless,

that plane determined from the initial phase has a dip direction/ dip angle of 145°/82°which is slightly different from the natural fault plane's one of 135°/60°. It may highlight that the initial phase also integrates some borehole deformation effects which are not included in this approach, *i.e.*, the borehole is not explicitly represented in the model.

Comparison in terms of flow rate at the injection point and pore pressure evolution at the monitoring point is presented in Fig. 16. The flow rate variation of the model behaves in a similar way to the experimental data (Fig. 16a). The injected flow rate is in the same order of magnitude during the period of crack propagation, *i.e.*, from 420 seconds to 450 seconds. The model predicts a very large increase in pore pressure at the monitoring point right after the fault reactivation, with a much higher pressure value (5.8 MPa) when compared to the data (3.4 MPa). It appears that the flow response is captured at the monitoring point when the pore pressure reaches 6.3 MPa at the injection point. For a rather short distance between injection point and monitoring point (1.5 m), the model predicts a lower pressure gradient (0.5 MPa) between these two locations, whereas a higher pressure gradient is observed in the data (2.9 MPa). This might highlight complexities in the flow paths connecting both boreholes. In *3DEC* no such complexities are introduced since flow between the two points is calculated using a simplified parallel plate model. The FM1 method is used for step 2 modeling where the admissible flow region is limited within a small range. The pressure response inside this range is evaluated synchronously even after the onset of crack propagation (see Fig. 10). Thus, a small difference in pore pressure between injection point and monitoring point is predicted by the model. It is possible that the flow model of the site could be a combination of FM1 (area very close to injection point) and FM2 (area away from the injection point). For such a case, the water leaks across the fault plane (or even through the rock matrix) when crack is propagated beyond the location of the monitoring point, yielding a lower pressure value.

Table 2. Fault orientation and stress tensor of Mont Terri data [24, 25], data used in a recent study [26] and data estimated in this study.

	Mont Terri stress tensor	Data used in Yves et al. [26]	Data estimated in this study
Fault dip/dip direction	60/135 (average)	60/135	82/145

σ_H (MPa)	4-5 (sub horizontal with dip direction of 310)	4.7±0.1 (dip direction 310±15)	5.8 (dip direction 330)
σ_h (MPa)	0.6-2.9 (sub horizontal with dip direction of 52)	3.8±0.1 (dip direction 40±15)	4.9 (dip direction 55)
σ_v (MPa)	6-7 (sub vertical)	5.5±0.1 (vertical)	5.7 (vertical)

Figure 12: rock displacement near the injection point from experiment data and fault orientation estimated from part 1 segment.

(a)   (b)

Figure 13: (a) stress orientation estimated from part 2 segment and (b) representation of initial fault stress on Coulomb slip envelope.
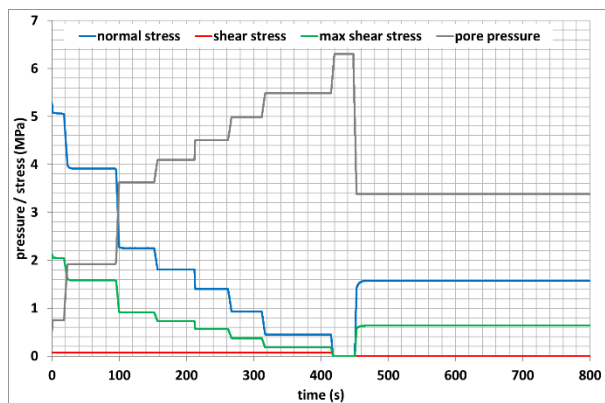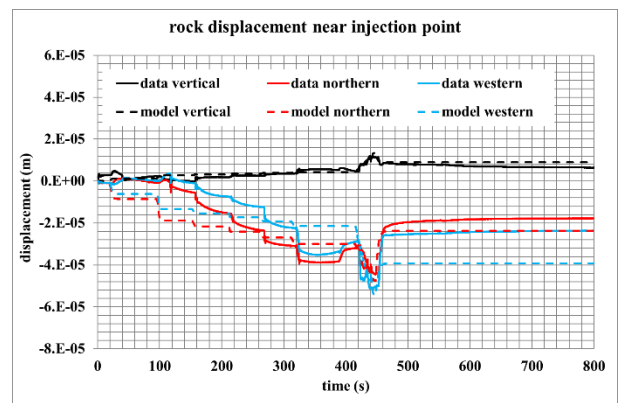
(a)   (b)

Figure 14: (a) stress evolution at the injection point and (b) comparison of displacement between numerical model and experimental data
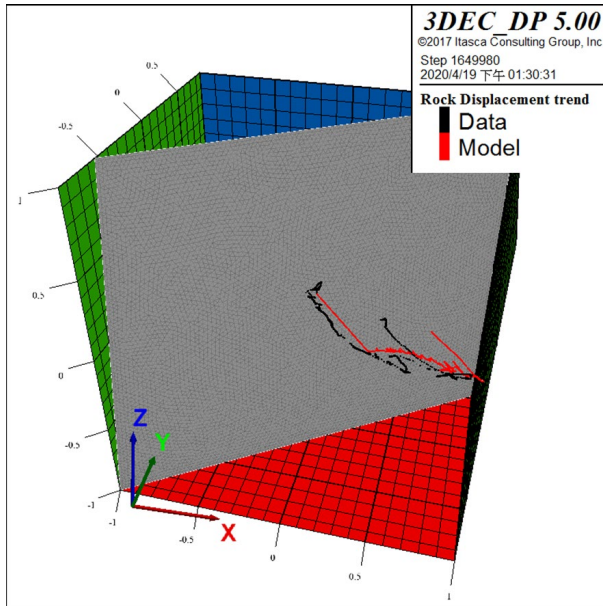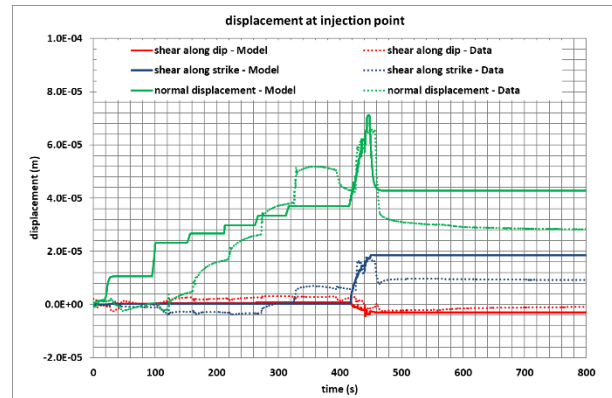
Figure 15: Comparison of rock displacement near the injection point (a) 3D visualization of displacement trend (b) fracture normal and shear displacement
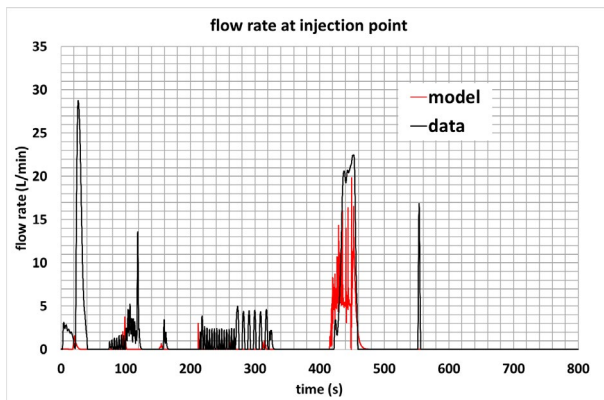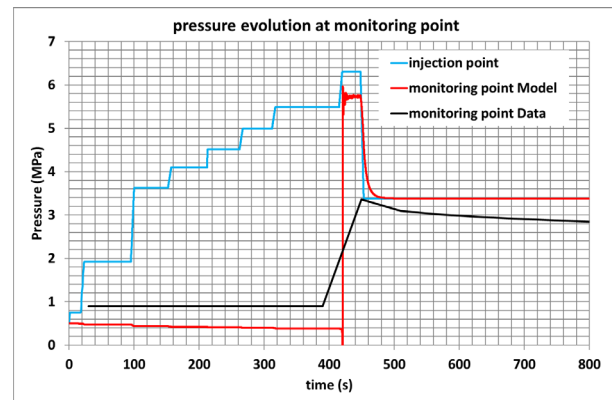
Figure 16: comparison of (a) flow rate and (b) pore pressure of monitoring point between numerical model and experimental data

5 CONCLUSIONS

The present study is aimed at reproducing the water injection induced fault slip in an argillaceous rock. A *3DEC* numerical model with a simple geometry is proposed to simulate the hydromechanical behavior of the fault during reactivation. The numerical configuration is based on the data obtained from experiments carried out at Mont Terri URL. The mechanical response of the joint

is modeled using a Coulomb slip criterion. Two joint flow models are compared for simulating hydraulic behavior of different nature of fault: fault initially non flowing (FM1) and fault initially flowing (FM2). It shows that as the injection pressure increases the effective stress near the injection point decreases leading to slip failure. Both models correctly predict the previous fault reactivation process, with different magnitudes of shear displacement. For the FM1 model, the injected water is accumulated near the injection point. A high pore pressure is developed before fault reactivation, and associated high leakage flowrate are suddenly observed, resulting in obvious shear displacements around the injection point. For the FM2 model, the increase in pore pressure is limited due to the water leakage through the entire flow plane. As a consequence, only a small amount of shear displacement is produced.

Our analyses show that the stress tensor can be estimated by coupled modeling of both the rock displacement and fluid pressure measured at the injection point. The trend of rock displacement induced by a step-wise water injection can be separated into 3 parts. The first part may correspond to a pure fault opening without any shear displacement, although it may be relatively inaccurate since this part occurs in the borehole stress perturbation zone. The second part indicates the extension of the rupture away from the borehole as we could associate it with a hydraulic connection with a monitoring borehole set meters away from the injection one. A rather high pore pressure is required to trigger the fault reactivation and significant shear displacement can be produced around the injection area, allowing to define a clear slip vector and to use it to estimate the shear stress on the activated surface. The last part is due to the pressure step- down inducing the normal displacement decrease, the reclosing of the fault and the arrest of shear slip. The fault orientation can be determined using the first part of the rock displacement. The normal vector of the fault should be in the same direction as the displacement lineament. This information when cross-checked with a post injection logging of the stimulated zone may allow the most probable activated plane to be identified. The in-situ stress can be estimated by using the second part of rock displacement and best fitting the in-situ stress tensor orientation and magnitude at the numerical model boundary. The best fit is when the direction of the resultant shear stress on the fault points in the same direction as the measured displacement trend of the second part. Moreover, the position of the initial joint stress state on the Coulomb failure diagram must lie in a reasonable horizontal distance with respect to the Coulomb slip envelope such that the fault reactivation can be triggered at a predictable water pressure. The present work shows a reasonable representation of a fully coupled fault reactivation process by using a rather simple model geometry. The model can be used to evaluate

the potential of a problematic fault slip by adjusting adequately the flow model between FM1 and FM2.

Further development is needed to improve the model behavior. In this paper, a single joint model is used for analyzing the induced fault reactivation and the associated coupling behavior between water pressure and rock joint. The injection conditions will be extended to account for multi fracture intersections. This can help to reveal the effect of water injection on reactivation process of surrounding joints and to see how these far field activations can eventually be captured at the injection by the SIMFIP probe. The proposed approach for *in-situ* stress estimation is mainly based on the rock displacement and the magnitude of the resultant joint stress with respect to Coulomb slip envelope. The qualified *in-situ* stress condition may not be unique. If a best-fit stress state locates along the FOP line (see Fig. 13b) and if the resultant joint stress satisfies the orientation requirement, then that particular *in-situ* stress should be able to reproduce similar model behavior. The development of mathematical solutions to previous *in-situ* stress estimation procedure is ongoing. The validation via numerical modeling will be performed to prove the reliability of the proposed stress estimation approach.

REFERENCES

[1] Min, K.-B., Lee, J., Stephansson O. Implications of thermally-induced fracture slip and permeability change on the long-term performance of a deep geological repository. International Journal of Rock Mechanics and Mining Sciences 2013;61:275–288. https://doi.org/10.1016/j.ijrmms.2013.03.009.

[2] Rutqvist J., Zheng L., Chen F., Liu H.-H., Birkholzer J. Modeling of Coupled Thermo-Hydro-Mechanical Processes with Links to Geochemistry Associated with Bentonite-Backfilled Repository Tunnels in Clay Formations. Rock Mechanics and Rock Engineering 2014;47: 167–186.

[3] Urpi L., Rinaldi A.P., Rutqvist J., Wiemer S. Fault stability perturbation by thermal pressurization and stress transfer around a deep geological repository in a clay formation. Journal of Geophysical Research: Solid Earth. 2019;124:8506–8518. https://doi.org/10.1029/2019JB017694.

[4] Lisle, R.J. & Srivastava D.C. 2004. Test of the frictional reactivation theory for faults and validity of fault-slip analysis, Geology, Vol. 32, No. 7, pp. 569-572.

[5] Rutqvist J., Birkholzer J., Cappa F., Tsang C.-F. Estimating maximum sustainable injection pressure during geological sequestration of CO2 using coupled fluid flow and geomechanical fault-slip analysis. Energy Conversion and Management 2007;48:1798–1807.

[6] Tsopela, A., Donzé, F. V., Guglielmi, Y., Castilla, R. & Gout, C. 2016. Hydro-mechanical modelling of hydraulic injection inside a fault zone, 50th US Rock Mechanics / Geomechanics Symposium in Houston, Texas USA 26-29 June, ARMA 16-476.

[7] Nguyen, T.S., Guglielmi, Y., Graupner, B. & Rutqvist, J. 2019. Mathematical modelling of Fault Reactivation Induced by Water Injection. Mineral, 9. 282.

[8] Itasca Consulting Group, Inc. 2013. *3DEC* – 3-Dimensional Distinct Element Code, Ver. 5.0. Minneapolis: Itasca.

[9] Birkholzer JT, Tsang CF, Bond AE, Hudson JA, Jing L, Stephansson O. 25 years of DECOVLEX - Scientific advances and lessons learned from an international research collaboration in coupled subsurface processes. International Journal of Rock Mechanics and Mining Sciences. 2019; 122: 103995.

[10] Rutqvist J, Graupner B, Guglielmi Y, Kim T, Maßmann J, Nguyen TS, Park JW, Shiu W, Urpi L, Yoon JS, Ziefle G, Birkholzer J. An international model comparison study of controlled fault activation experiments in argillaceous claystone at the Mont Terri Laboratory. Int J Rock Mech Min Sci. (this issue, under review, submission no: IJRMMS_2020_494)

[11] Guglielmi, Y., Elsworth, D., Cappa, F., Henry, P. Gout, C., Dick, P. & Durand, J. 2015. In-situ observations on the coupling between hydraulic diffusivity and displacements during fault reactivation in shales, J. Geophys. Res. Solid Earth, Vol. 120, No. 11, pp. 7729-7748.

[12] Guglielmi, Y., Birkholtzer, J., Rutqvist, J., Jeanne, P., & Nussbaum, C. 2017. Can Fault leakage occur before or without reactivation? Results from an in-situ reactivation at Mont Terri. Energy Procedia, 114, 3167-3174.

[13] Guglielmi, Y., Nussbaum, C., Jeanne, P., Rutqvist, J., Cappa, F., & Birkholzer, J. (2020). Complexity of fault rupture and fluid leakage in shale: Insights from a controlled fault activation experiment. Journal of Geophysical Research: Solid Earth, 125, e2019JB017781. https://doi.org/ 10.1029/2019JB017781.

[14] Haimson B., Cornet F. ISRM Suggested Methods for rock stress estimation—Part 3:hydraulic fracturing (HF) and/or hydraulic testing of pre-existing fractures (HTPF). Int. J. Rock mechanics & Mining Sciences 40, 2003, 975-989.

[15] Ljunggren C., Chang Y, Jason T, Christiansson R. An overview of rock stress measurement methods. Int. J. Rock mechanics & Mining Sciences 40, 2003, 1011-1020.

[16] Amadaei B, Stephansson O. Rock stress and its measurement. London: Chapman & Hall; 1997.

[17] Cornet FH, Valette B. Insitu stress determination from hydraulic injection test data. J Geophys Res 1984;89:11527-37.

[18] Rutqvist J. and Stephansson O. Cyclic hydraulic jacking to determine virgin stress normal to a fracture. International Journal of Rock Mechanics and Mining Sciences & Geomechanical Abstracts, 33, 695-711 (1996).

[19] Ljunggren C. Rock stress measurements by means of hydraulic method at Hästholmen, 1998-1999. Working Report 99-54, Posiva Oy, Finland, 1999. 63pp.

[20] Bjarnason B, Raillard G. Rock stress measurements in borehole V3 Stripa Project 87-13. Swedish Nuclear Fuel and Waste Management Co., 1987. 40pp.

[21] Ljunggren C, Raillard G. In-situ stress determination by hydraulic tests on pre-existing fractures at Gideå test site, Sweden Research Report TULEA 1986:22, Luleå University, Sweden 1986. 77pp.

[22] Guglielmi, Y., Cappa, F., Lançon, H., Janowczyk, J. B., Rutqvist, J., Tsang, C. E., & Wang, J. S. Y. 2013. ISRM Suggested Method for Step-Rate Injection Method for Fracture In-Situ Properties (SIMFIP): Using a 3-Components Borehole Deformation Sensor. Rock Mech. Rock. Eng. 47, 303-311.

[23] Witherspoon, P.A., Wang J.S.Y., Iwai, K., & Gale, J.E. 1980. Validity of Cubic Law for Fluid Flow in a Deformable Rock Fracture. Water Resource Res., 16(6), 1016-1024.

[24] Corkum AG, Martin CD. Modelling a mine-by test at the Mont Terri rock laboratory, Switzerland. Int J Rock Mech Min Sci. 2007;44:846–859.

[25] Amann F., LeGonidec Y., Senis M., Gschwind S., Wassermann J., Nussbaum C., Sarout J. Analysis of acoustic emissions recorded during a mine-by experiment in an underground research laboratory in clay shales. International Journal of Rock Mechanics and Mining Sciences 2018;106:51–59.

[26] Guglielmi, Y., Nussbaum, C., Rutqvist, J., Cappa, F., Jeanne, P. and Birkholer, J. Estimating perturbed stress from 3-D borehole displacements induced by fluid injection in fractured or faulted shales. *Geophys. J. Int.* (2020) 221, 1684-1695.